Bull. Chem. Soc. Ethiop. **2027**, 41(1), 99-118.
DOI: https://dx.doi.org/10.4314/bcse.v41i1.8

ISSN 1011-3924
Printed in Ethiopia
Online ISSN 1726-801X
© 2027 Chemical Society of Ethiopia and The Authors

INTEGRATIVE DFT, DOCKING, AND ADMET EVALUATION OF A PROMISING SCHIFF BASE INHIBITOR (DMBI) FOR TUBERCULOSIS THERAPY

Efdal Çimen[1], Gül Kotan[1*], Kenan Gören[2], Veysel Tahiroğlu[3]

[1]Kafkas University, Department of Chemistry and Chemical Processing Technologies, Vocational School, Kars, Türkiye
[2]Şırnak University, Faculty of Engineering, Department of Petroleum and Natural Gas Engineering, Şırnak, Türkiye
[3]Nursing Department, Health Sciences Faculty, Şırnak University, Şırnak, Türkiye

(Received February 20, 2026; Revised June 1, 2026; Accepted September 30, 2026)

ABSTRACT. Tuberculosis continues to pose a serious global health threat due to the increase in drug-resistant *Mycobacterium tuberculosis* strains. In this study, the activity of (Z)-3-(((E)-4-(dimethylamino)benzylidene)hydrazinylidene)indolin-2-one (DMBI), a Schiff base derivative, as a potential inhibitor of tuberculosis was investigated. The molecular structure of DMBI was optimized using the B3LYP/B3PW91 methods and the 6-311G(d,p) basis set within the scope of density functional theory (DFT); the HOMO-LUMO energy gap, molecular electrostatic potential distribution, Mulliken atomic charges, and intramolecular interactions were analyzed in detail. Preliminary orbital analyses showed that the molecule exhibits significant nonlinear optical properties. Molecular docking studies with tuberculosis enzymes (PDB: 1SJ2 and 4P8N) revealed strong interactions with binding affinities of -9.7859 and -8.1283 kcal/mol, respectively. ADMET evaluations indicate that DMBI has a suitable pharmacokinetic and toxicological profile for drug development. The findings suggest that DMBI may serve as a potential anti-tuberculosis lead compound; however, further experimental and biological validation studies are required to confirm its therapeutic efficacy.

KEY WORDS: Tuberculosis, Schiff base, DFT, HOMO-LUMO, Molecular docking

INTRODUCTION

Tuberculosis (TB), caused by Mycobacterium tuberculosis, is a serious infectious disease that can affect many organs, especially the lungs. Transmitted through the respiratory tract, TB can spread rapidly, particularly in crowded and poorly ventilated environments [1]. Individuals with weakened immune systems, such as those with diabetes, HIV/AIDS, or malnutrition, are at increased risk of infection [2]. In recent years, multidrug-resistant tuberculosis (MDR-TB), which is resistant to standard first-line treatments, has posed a serious threat to global public health [3]. While existing preventive and treatment strategies, particularly the BCG vaccine and long-term antibiotic therapy, play a critical role in disease control, factors such as delayed diagnosis, inadequate healthcare infrastructure, and non-adherence to treatment contribute to the persistence of TB in many regions. This situation necessitates the development of new and effective therapeutic agents [4].

Schiff bases are organic compounds containing a carbon–nitrogen double bond (-CH=N-) formed through nucleophilic addition reactions between aldehydes or ketones and amines. Aldehyde–amine reactions yield azomethine (aldimine) compounds, whereas ketone–amine reactions produce imine (ketimine) derivatives [5]. Due to their chemical stability, ease of synthesis, and broad spectrum of biological activities, Schiff bases have attracted considerable attention in both fundamental and applied chemistry, as well as pharmaceutical research [6]. Their ability to form metal complexes provides significant advantages in coordination chemistry and catalysis, while their antibacterial, antifungal, antiviral, and anticancer activities highlight their

*Corresponding author. E-mail: gulkemer@hotmail.com
This work is licensed under the Creative Commons Attribution 4.0 International License

potential for pharmaceutical applications [2, 7, 8]. Furthermore, Schiff bases are widely utilized in advanced technological applications, including sensor design, organic light-emitting diodes (OLEDs), and molecular magnetic materials [9].

Despite the growing interest in Schiff base derivatives as biologically active molecules, studies focusing on indolin-2-one-based Schiff base compounds against tuberculosis-related molecular targets remain limited. In particular, the structural and electronic characteristics of (Z)-3-(((E)-4-(dimethylamino)benzylidene)hydrazinylidene)indolin-2-one (DMBI), including its potential interactions with tuberculosis-associated enzymes, have not yet been comprehensively investigated using integrated quantum chemical and molecular modeling approaches. Moreover, the coexistence of indolin-2-one and dimethylaminobenzylidene moieties in the DMBI structure may contribute to enhanced electronic delocalization, intermolecular interaction capability, and pharmacological potential. Therefore, a detailed theoretical investigation of DMBI may provide valuable preliminary insights for anti-tuberculosis drug discovery and future experimental validation studies.

Density functional theory (DFT) is a widely used quantum chemical approach for investigating the electronic structure, reactivity, and intermolecular interactions of molecules [10]. Parameters such as HOMO–LUMO energy gaps, molecular electrostatic potential distributions, and Mulliken atomic charges provide crucial insights into the chemical stability and interaction potential of molecules [11]. In addition, the photophysical and electronic properties of molecules can be evaluated through electron density distribution analyses using Natural Bond Orbital (NBO) analysis, as well as nonlinear optical (NLO) investigations [12]. Previous studies have emphasized the critical role of DFT analyses in predicting the reactivity and potential biomolecular interactions of novel drug candidates [13].

Molecular docking is an in silico technique used to predict the binding mode and binding affinity of a ligand toward a target protein [2]. This method serves as an effective tool for identifying potential inhibitors and understanding ligand–protein interactions in drug design studies. Docking analyses guide experimental biological investigations by evaluating interaction types such as hydrogen bonding, hydrophobic interactions, and π–π stacking [14]. The literature indicates that combining DFT and docking results with ADMET (Absorption, Distribution, Metabolism, Excretion, and Toxicity) analyses provides a comprehensive preliminary assessment of the efficacy and safety profiles of candidate molecules [15]. ADMET predictions are highly valuable for guiding advanced experimental studies by providing early insights into the pharmacokinetic and toxicological properties of molecules [16].

In light of the limited studies on DMBI-based Schiff base derivatives against tuberculosis-related targets, this study aims to provide a comprehensive theoretical investigation of the structural, electronic, and pharmacological properties of (Z)-3-(((E)-4-(dimethylamino)benzylidene)hydrazinylidene)indolin-2-one (DMBI) [17] The molecular structure and electronic properties of DMBI were optimized using DFT calculations, and detailed analyses were carried out, including HOMO–LUMO energy gap analysis, molecular electrostatic potential mapping, Mulliken atomic charge analysis, NBO analysis, and NLO analysis. Furthermore, molecular docking studies were performed to evaluate its interaction potential toward TB-related enzymes, while ADMET analyses were conducted to investigate its pharmacokinetic and toxicological properties. The findings are intended to provide a theoretical framework for future biological validation studies and to evaluate whether DMBI may represent a potential lead compound against tuberculosis rather than directly claiming therapeutic applicability.

EXPERIMENAL

In this study, the DMBI molecule was designed in ChemBioDraw software and prepared to form the basis of quantum chemical calculations. The initial geometry of the molecule was optimized

using the SYBYL2 (mol2) method in the Chem3D environment. The obtained 3D structures were converted to MOL2 format and imported into Gaussian 09 [18] via the GaussView 6.0 interface. Geometry optimization of DMBI was performed using density functional theory (DFT) with the B3LYP and B3PW91 functionals in combination with the 6-311G(d,p) basis set. Frequency calculations were additionally carried out at the same level of theory to confirm that the optimized geometry corresponds to a true energy minimum (no imaginary frequencies). After optimization, structural parameters such as bond lengths and bond angles were analyzed. Electronic properties including HOMO–LUMO energy gap, Mulliken atomic charge distribution, molecular electrostatic potential (MEP), Natural Bond Orbital (NBO) interactions, and nonlinear optical (NLO) properties were evaluated based on the optimized wavefunction. Molecular docking analyses were carried out using the AutoDock Vina software [19] to determine the interaction of DMBI with potential biological targets. In this context, crystal structures of target proteins were obtained from the Protein Data Bank (PDB ID: 1SJ2 and 4P8N) [20, 21]. Protein structures were retrieved from the Protein Data Bank and prepared by removing water molecules, adding polar hydrogen atoms, and assigning Kollman charges. To ensure the reliability and reproducibility of the docking protocol, a validation procedure was performed by redocking the co-crystallized ligand into the active site of the target proteins. The accuracy of the docking method was evaluated by calculating the root mean square deviation (RMSD) between the experimental and predicted ligand poses, confirming the reliability of the docking protocol. The docking grid box was defined based on the coordinates of the co-crystallized ligand to ensure proper coverage of the active binding site. Grid center coordinates were selected according to the active site residues, and grid dimensions were adjusted to include all key interacting amino acids involved in ligand binding. Docking calculations were performed with sufficient sampling of ligand conformations to ensure reliable binding mode predictions. Binding affinities and interaction profiles, including hydrogen bonds, hydrophobic interactions, and π–π stacking, were analyzed in detail. Visualization of docking poses was carried out using Discovery studio 2016 [22] software. In addition, pharmacokinetic properties, drug similarity criteria, biological activity scores, and ADMET (absorption, distribution, metabolism, excretion, and toxicity) parameters for the DMBI complex were predicted in silico using the Admetlab 2.0 online platform [23].

RESULTS AND DISCUSSION

Structure details and analysis

Geometric analysis allows the determination of bond lengths, angles, and symmetry properties of molecules, while geometric optimization aims to obtain the most stable structure [24]. This approach is critical for understanding the structural and electronic properties of molecules in fields such as drug design, catalysis research, and materials science [25]. The optimized geometry of the DMBI molecule has been presented in Figure 1, while the calculated bond lengths and bond angles obtained using two density functional theory approaches are summarized in Table S1. Carbon–carbon bond lengths range from 1.378 to 1.460 Å, indicating the aromatic nature of the molecular framework and partial double-bond character. The C–N and N–N bonds within the nitrogen-containing region are approximately 1.371–1.396 Å, respectively, suggesting the influence of electron delocalization. The carbonyl C=O bond length is approximately 1.213 Å, which is consistent with typical carbonyl bond distances reported in similar systems. The bond angles within the aromatic rings vary between 117° and 121°, suggesting that the molecule maintains an approximately planar arrangement. The angles involving heteroatoms, such as C4–N7–C8 (112.8°) and N7–C8–O10 (124.6°), indicate localized electronic effects around these atomic centers. Most dihedral angles are close to ±180°, supporting a predominantly planar molecular configuration, whereas several values around 60° may be attributed to localized steric interactions and limited rotational flexibility. Only minor differences were observed between the

computational methods, indicating a generally consistent structural description of the DMBI molecule. These findings suggest structural stability and preservation of molecular planarity, which may influence the electronic characteristics of the compound. The calculated bond lengths and bond angles of the DMBI molecule show good agreement with previously reported crystal structures of hydrazono-indolin-2-one derivatives. The aromatic C–C bond lengths in the indolin-2-one ring (1.38–1.42 Å) are comparable to the values reported for (3Z)-3-hydrazinylideneindolin-2-one by Jamal *et al.* [26]. The C=N bond of the hydrazono group (1.29 Å) falls within the range commonly reported for hydrazone-containing compounds and is consistent with values reported by Jamal *et al.* [26] and Halasangi *et al.* [27]. Similarly, the N–N bond length of the hydrazono system (1.36–1.38 Å) is compatible with literature data reported for related derivatives [27, 28]. Regarding bond angles, the C2–C3–C4 and C4–C5–C6 angles calculated for DMBI are in the range of 118–121°, which is consistent with the expected sp^2 hybridization of the indolin-2-one framework and comparable to reported crystallographic findings [26]. The N–N–C and N–C–C bond angles in the hydrazono region generally range from 111° to 122°, showing agreement with both experimental crystal structures and theoretical studies reported for similar compounds [27, 28]. Overall, the optimized geometry of DMBI is consistent with the structural characteristics reported for related hydrazono-indolin-2-one systems.

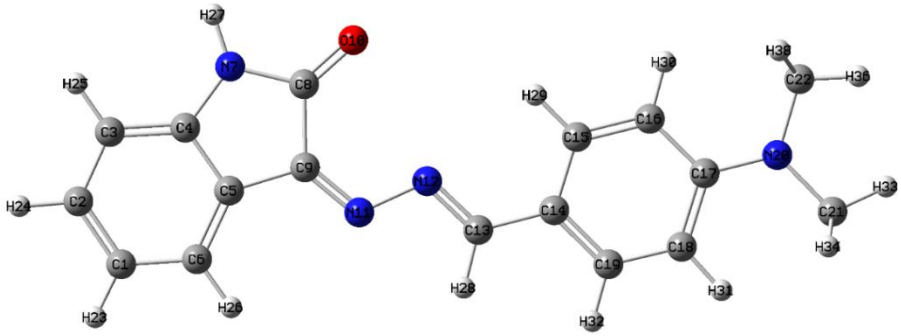


Figure 1. Optimized molecular geometry of the DMBI molecule calculated at the B3PW91/6-311G(d,p) level of theory in the gas phase.

Mulliken atomic charges

Mulliken atomic charge analysis is a computationally efficient approach used to estimate atomic charges by distributing electron density among atoms within a molecule [29]. This method provides a qualitative evaluation of electron distribution based on molecular orbital coefficients and may help identify electron-rich and electron-deficient regions, possible reactive sites, and interaction tendencies [30]. The Mulliken atomic charges of the DMBI molecule have been presented in Table S2, allowing a detailed evaluation of the molecular charge distribution. Examination of the Mulliken atomic charges of DMBI reveals a heterogeneous electron density distribution across the molecular framework. Carbon atoms exhibit both positive and negative charge values depending on their chemical environment; C4 and C8 display relatively pronounced positive charges, whereas atoms such as C1, C2, C3, C15, C16, and C19 possess slightly negative charges. This variation suggests nonuniform electron density across different regions of the molecule. Nitrogen and oxygen atoms show relatively high negative charge densities, indicating electron-rich regions that may act as potential nucleophilic sites. In particular, N7 carries the highest electron density and may represent an important region in terms of molecular reactivity. Similarly, N20 and O10 exhibit notable negative charge accumulation, suggesting possible interaction-prone regions. Other heteroatoms, including N11, N12, and O18, also contribute to

electron density, although to a lesser extent. Hydrogen atoms generally possess positive charges, with H27 and H37–H38 exhibiting comparatively higher positivity, which may favor their participation as potential hydrogen bond donors. Overall, DMBI exhibits a heterogeneous electronic distribution, where negatively charged nitrogen and oxygen atoms may contribute to nucleophilic behavior, while positively charged carbon and hydrogen atoms may represent electron-deficient regions with possible interaction potential. Although small differences between computational methods may affect the magnitude of atomic charges, the general charge distribution trend remains consistent, reflecting the electronic characteristics of the molecular framework.

Docking studies demonstrated favorable binding conformations of DMBI with Mycobacterium tuberculosis enzymes (PDB: 1SJ2 and 4P8N). Protein Data Bank In this context, the charge distribution obtained from Mulliken analysis may provide complementary theoretical insight into possible electrostatic interaction regions within protein binding pockets. However, these findings should be interpreted cautiously, as Mulliken atomic charges alone do not directly confirm biological activity. Instead, they provide supportive information for understanding possible molecular interaction tendencies and may contribute to future structural optimization studies.

Frontier molecular orbital analysis

Molecular orbital theory provides a critical theoretical framework for understanding the chemical and physical properties of a molecule [31]. Within this framework, the highest-energy occupied molecular orbital (HOMO) and the lowest-energy unoccupied molecular orbital (LUMO), called frontier molecular orbitals (FMOs), play a fundamental role in determining the electron behavior of a molecule. The interaction between HOMO and LUMO generally leads to $\pi \rightarrow \pi^*$ electronic transitions, which directly affect the optical and photochemical properties of molecules [32]. Furthermore, the HOMO–LUMO energy difference, also known as the energy gap, is a key indicator of a molecule's chemical reactivity and kinetic stability. Molecules with a small energy difference are considered "soft" due to their high reactivity and low kinetic stability, while molecules with a large energy gap are considered more stable and less reactive [33]. The HOMO and LUMO energy values of the DMBI molecule, calculated using two different methods, provide insights into its electronic structure and reactivity (Table 1). The negative HOMO and positive LUMO energy values obtained from both methods indicate that electron donation is energetically more favorable than electron acceptance. The calculated energy gap (ΔE) of approximately 7 eV suggests that DMBI exhibits relatively high kinetic stability and low chemical reactivity. The difference between ionization potential (I) and electron affinity (A) further supports a greater tendency toward electron donation compared to electron acceptance.

While chemical hardness (η) and softness (s) values indicate a relatively hard and less reactive character, the chemical potential (μ) and electronegativity (χ) values suggest limited electron-accepting ability. Similarly, the electrophilicity index (ω) values indicate relatively low electrophilic character, suggesting a stable electronic configuration under isolated conditions.
It should be noted that these global reactivity descriptors provide information about the intrinsic electronic properties of the molecule; however, they do not directly demonstrate biological activity. Therefore, any relationship with inhibitory potential should be interpreted cautiously. In this context, the calculated electrophilicity index (ω: 1.08–1.10 eV) and chemical potential (μ:–2.76 eV) values may reflect a favorable electronic profile for intermolecular interactions, but they do not constitute direct evidence of biological efficacy.

Instead, these electronic features can be considered as complementary information when evaluated together with molecular docking results against Mycobacterium tuberculosis targets (PDB: 1SJ2 and 4P8N), rather than as standalone proof of binding or inhibition. Overall, the results obtained from two different computational methods show consistent trends regarding the

electronic structure and stability of the DMBI molecule. The HOMO and LUMO orbitals were obtained using Equations 1-6. Figure 2 illustrates the frontier molecular orbitals of the DMBI molecule and the corresponding electron density distribution. These orbitals clearly show regions of electron density localization within the molecular framework.

$$\Delta E = |E_{HOMO} - E_{LUMO}| \quad (1)$$

$$\eta = (I - A)/2 \quad (2)$$

$$s = \frac{I}{\eta} \quad (3)$$

$$\mu = \frac{(I+A)}{2} \quad (4)$$

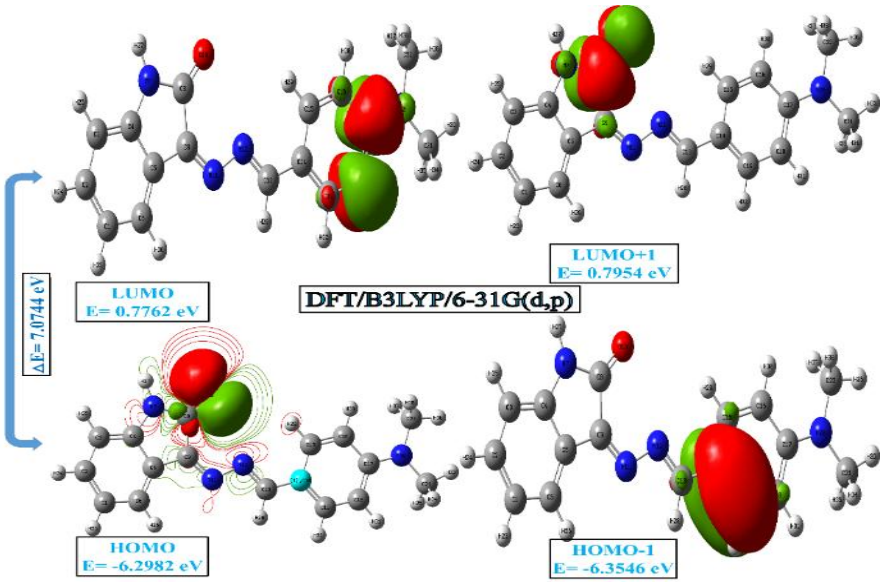
$$\chi = -(I + A)/2 \quad (5)$$

$$\omega = \mu^2/2\eta \quad (6)$$

Table 1. HOMO and LUMO energy values and related global reactivity descriptors of the DMBI molecule calculated using the B3LYP and B3PW91 methods.

	E_{HOMO}	E_{HOMO-1}	E_{LUMO}	E_{LUMO+1}	ΔE	I	*A*	η	*s*	μ	χ	ω
B3LYP	-6.2982	-6.3546	0.7762	0.7954	7.0744	6.2982	-0.7762	3.5372	0.283	-2.761	2.761	1.077
B3PW91	-6.3524	-6.2222	0.7512	0.7692	7.1036	6.3524	-0.7512	3.5518	0.282	-2.801	2.801	1.103

ΔE→Energy Gap, I→Ionization Potential($-E_{HOMO}$), *A*→Electron Affinity($-E_{LUMO}$), η→Chemical hardness, *s*→Chemical softness, μ→Chemical



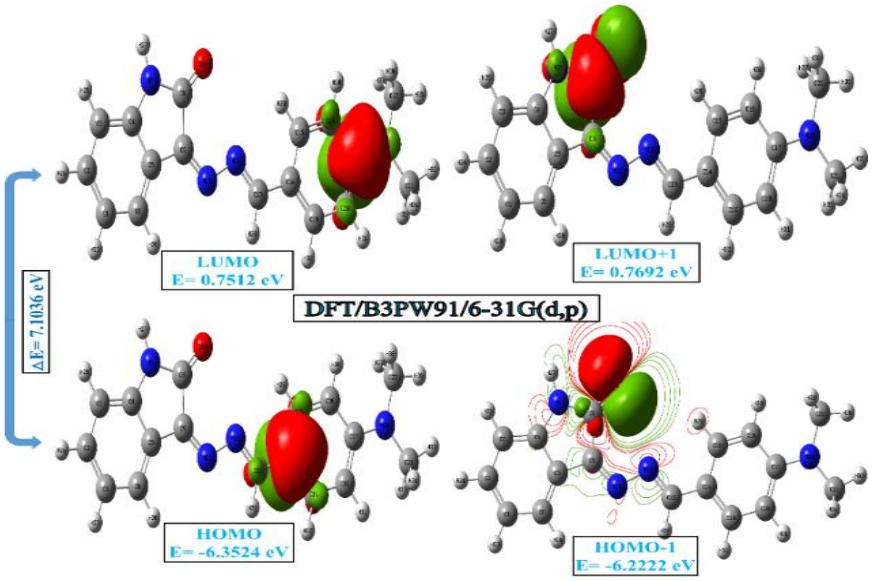


Figure 2. Frontier molecular orbitals (HOMO and LUMO) of the DMBI molecule calculated using the B3LYP and B3PW91 methods.

Molecular electrostatic potential (MEP)

Molecular electrostatic potential (MEP) surface analysis is a technique that allows the electrostatic potential of a molecule to be mapped onto its isoelectron density surface, providing information about reactive sites [34]. This method simultaneously visualizes the molecule's size, shape, and electrostatic potential distribution. According to the color scheme used, red regions represent electron-rich and partially negatively charged areas, while blue regions represent electron-poor and partially positively charged areas [35]. Light blue represents slightly electron-poor regions, yellow represents slightly electron-rich regions, and green represents neutral regions. Furthermore, in most MEP maps, the maximum positive region most susceptible to nucleophilic attack is marked in blue, while the maximum negative region most susceptible to electrophilic attack is marked in red [36].

The MEP, TD (Time-Dependent), MESP (Molecular Electrostatic Surface Potential) 3D+2D, and contour maps of the DMBI molecule (Figure 3) illustrate its electrostatic potential distribution under two different DFT functionals (B3LYP and B3PW91). Both methods show a similar overall distribution pattern of electrostatic potential across the molecular surface. The contour maps further indicate localized variations in potential around specific atomic regions, while the 3D surfaces highlight spatial charge distribution. Among the two functionals, B3PW91 provides slightly more pronounced potential gradients; however, the overall qualitative features remain consistent. The calculated electrostatic potential range is -6.978×10^{-2} to $+6.978\times10^{-2}$ for B3LYP and -6.988×10^{-2} to $+6.988\times10^{-2}$ for B3PW91 at the 6-311G(d, p) basis set level, indicating comparable electronic descriptions from both methods. The negative potential region is mainly localized around the O10 atom, suggesting it as an electron-rich site, while positive potential regions are observed near the N22 atom, indicating electron-deficient character in this region. These results provide qualitative insight into possible intermolecular interaction sites of the DMBI molecule. However, MEP analysis alone does not directly predict biological activity or binding strength. Therefore, any relationship with ligand–protein interactions should be interpreted in

combination with molecular docking results rather than as direct evidence. In this context, the identified electrostatic features may help explain the preferred orientation of DMBI within the binding pockets of Mycobacterium tuberculosis target proteins (PDB: 1SJ2 and 4P8N), as also suggested by docking simulations. Overall, MEP analysis indicates a non-uniform charge distribution that may influence intermolecular interaction tendencies, while remaining a qualitative descriptor of electronic structure rather than a direct measure of biological efficacy.

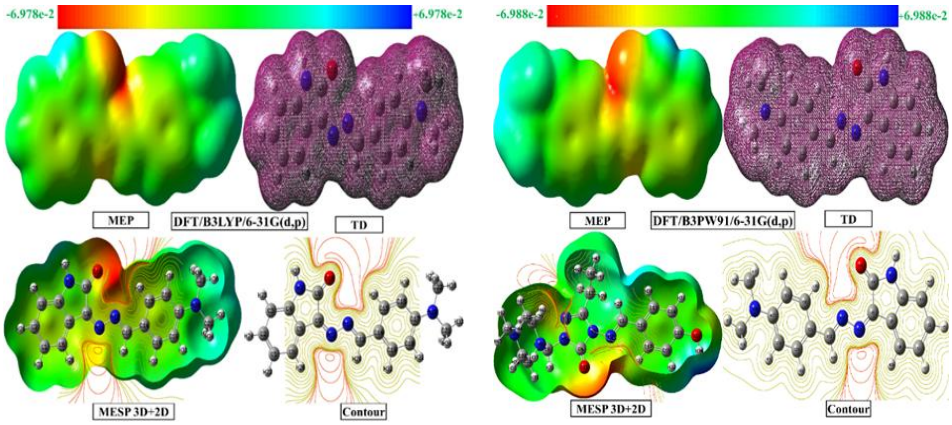


Figure 3. Three-dimensional (3D) and two-dimensional (2D) molecular electrostatic potential (MEP) surfaces, time-dependent (TD) analysis results, and molecular electrostatic surface potential (MESP) contour maps of the DMBI molecule calculated using the B3LYP and B3PW91 methods.

Non-linear optical properties (NLO)

Nonlinear optical (NLO) properties are of increasing importance in communication technologies, signal processing, optical interconnects, optical memory, and optical modulation. These properties play a critical role in the development of telecommunications and optical computing technologies and have become a major focus of researchers [37]. The response of a molecule to an electric field underlies nonlinear optical behavior. In particular, the nonlinear optical response of an isolated molecule under an electric field Ei(x) can be expressed by a Taylor series expansion over the field-induced total dipole moment μtot. This approach provides a critical method for understanding the polarization properties and higher-order optical responses of molecules [38].

$$\alpha_{\text{tot}} = \mu_0 + \alpha_{ij}E_J + \beta_{ijk}E_{Jk} + \ldots \quad (7)$$

In this study, the B3LYP and B3PW91 hybrid density functional methods combined with the 6-311G(d,p) basis set were selected for NLO calculations due to their well-documented reliability in predicting electronic and optical properties of organic molecules. B3LYP is widely used because it provides a balanced description of exchange–correlation effects and has been shown to yield accurate geometrical and electronic parameters for conjugated systems. On the other hand, B3PW91 is known for its improved treatment of exchange interactions, which can offer complementary insights into molecular polarizability and hyperpolarizability values. The 6-311G(d,p) basis set was chosen to ensure an adequate description of electron distribution and polarization effects, which are essential for reliable NLO property estimation. The use of these

methods together allows for a more robust and comparative evaluation of the nonlinear optical responses of the DMBI molecule. Non-Linear Optical (NLO) properties of the DMBI molecule were evaluated through the calculation of dipole moment (μ), polarizability (α), and first hyperpolarizability (β) using the B3LYP and B3PW91 methods with the 6-311G(d,p) basis set, and the results have been presented in Table 2. The calculated data indicate that the net dipole moment of the molecule has a moderate magnitude and is predominantly oriented along the x-axis (B3LYP: 3.702 D, B3PW91: 3.858 D). The μy and μz components are negligibly small, suggesting that the molecular structure results in an anisotropic charge distribution with a preferred polarization direction. The average polarizability (α_total) values were found to be similar for both methods (B3LYP: 104.41 au, B3PW91: 103.16 au), indicating a consistent linear optical response. This suggests that the electron cloud can be moderately distorted under an external electric field. The first hyperpolarizability (β_total) values are also comparable for both computational methods (B3LYP: 1.782×10^{-30} esu, B3PW91: 1.785×10^{-30} esu), indicating a stable nonlinear optical response. In particular, the dominance of the βxxx component suggests that the nonlinear optical activity is mainly directed along the x-axis. Overall, these results indicate that the DMBI molecule exhibits an asymmetric electronic structure, contributing to its dipole moment and nonlinear optical response. However, these findings are interpreted solely in terms of electronic and optical properties, without extending the discussion to biological activity. For comparison, the calculated μ, α, and β values of DMBI were evaluated against those of urea as a reference molecule. The dipole moment of DMBI is higher than that of urea, indicating stronger intramolecular charge separation. Similarly, the polarizability and first hyperpolarizability values are higher than those of urea, indicating enhanced electronic deformability and nonlinear optical response. The μ, α, and β values obtained at the B3LYP and B3PW91 levels indicate that DMBI has a moderately polar character and enhanced electron cloud deformability. These results are presented strictly as theoretical NLO and electronic structure analysis. NLO values were calculated using Equations (8–11).

$$\mu = \left(\mu_x^2 + \mu_y^2 + \mu_z^2\right)^{1/2} \tag{8}$$

$$\alpha_{\text{Total}} = \frac{1}{3}(\alpha_{xx} + \alpha_{YY} + \alpha_{zz}) \tag{9}$$

$$\beta_{Total} = (\beta^2 x + \beta^2 y + \beta^2 z)^{1/2} \tag{10}$$

$$(\beta xxx + \beta xyy + \beta xzz)^2 + (\beta yyy + \beta yxx + yzz)^2 + (\beta zzz + \beta zxx + \beta zyy)^2]^{\frac{1}{2}} \tag{11}$$

Table 2. Dipole moment (Debye), polarizability (a.u.), tensor components, and total values of the DMBI molecule calculated using the B3LYP and B3PW91 methods with the 6-311G(d,p) basis set.

Parameters	B3LYP	B3PW91	Parameters	B3LYP	B3PW91
μ_x	3.6742	3.8324	β_{XXX}	184.7377	189.8445
μ_y	-0.4533	-0.4421	β_{YYY}	5.7583	4.7378
μ_z	0.0005	0.0000	β_{ZZZ}	0.0006	-0.0007
$\mu_{(D)}$	3.7020	3.8578	β_{XYY}	-4.1991	-4.2273
αxx	-65.1729	-62.9111	β_{XXY}	56.0628	56.5120
α_{YY}	-117.1376	-115.5086	β_{XXZ}	0.0111	0.0126
αzz	-130.9191	-131.0668	β_{XZZ}	7.9496	8.9912
α_{XY}	-3.7287	-3.7738	β_{YZZ}	8.1046	8.2831
α_{XZ}	-0.0004	-0.0025	β_{YYZ}	0.0019	0.0024
α_{YZ}	0.0000	0.0001	β_{XYZ}	-0.0061	-0.0104
α(au)	−104.41	−103.16	β(esu)	1.782×10^{-30}	1.785×10^{-30}

NBO analysis

Natural bonding orbital (NBO) analysis is an effective method for the detailed study of intra- and intermolecular interactions in molecular systems, particularly for the quantitative assessment of charge transfer processes and conjugative and hyperconjugative interactions [39]. The integrated treatment of occupied (donor) and virtual (acceptor) orbital spaces allows the identification of fundamental electronic rearrangements that contribute to molecular stability. In this study, donor-acceptor orbital interactions are analyzed within the context of second-order perturbation theory based on Fock matrix elements [40]. For a more meaningful interpretation, only interactions that provide stabilization energies of $E(2)\geq10$ kcal mol^{-1} are considered.

$$E(2) = q_i.F(i,j)^2 / (\varepsilon_i-\varepsilon_j) \quad (12)$$

Natural Bond Orbital (NBO) analysis provides information on electron delocalization and stabilization energies and enables identification of reactive centers via atomic charge distribution. Negative and positive charges indicate nucleophilic and electrophilic sites, respectively, which are important for intermolecular interactions. Previous studies have shown that NBO-derived charges can be used to interpret protein–ligand interactions in docking studies. Therefore, the charge distribution in DMBI supports its docking interaction analysis [41]. The second-order perturbation energy values (E(2)) given in Table 3 indicate that the π→π* transitions, particularly those located in the aromatic nucleus, contribute significantly to the electronic stabilization of the molecule. π→π* interactions in the range of 16–23 kcal/mol observed at the C1–C2, C3–C4, and C5–C6 double bonds forming the aromatic backbone are indicative of strong conjugation. Among these interactions, the C3–C4(π)→C5–C6(π)* transfer provides the highest stabilization with 23.13 kcal/mol, demonstrating an effective resonance interaction between adjacent π-systems. Furthermore, the C3–C4(π)→C5–C6(π)** interaction between antibonding orbitals has an exceptionally high E(2) value, indicating that orbital energy proximity and electron density distribution in this region support a strong π-conjugation framework. Most of the σ→σ* transitions are between 4–6 kcal/mol, representing the typical hyperconjugative stabilization of the carbon skeleton. The C1–C6(σ)→C5–C9(σ)**, C2–C3(σ)→C4–N7(σ), and C5–C6(σ)→C5–C9(σ)* interactions indicate electron delocalization between the carbon framework and the heteroatom-containing segment. Such interactions are inherent hyperconjugative processes that contribute to the geometric and electronic stabilization of the molecule. The heteroatom-containing regions, especially the C9–N11, N12–C13, and C8–O10 bonds, are also noteworthy. The N12–C13(π)→C9–N11(π)* (18.66 kcal/mol) and C9–N11(π)→N12–C13(π)* (12.36 kcal/mol) interactions indicate a strong bidirectional resonance interaction in this segment. In addition, the C8–O10(π)→C9–N11(π)* interaction supports the participation of the oxygen atom in the π-system and conjugative coupling with the adjacent C–N bond. Similarly, the C9–N11 π→N12–C13 π* transition (E(2)=12.36 kcal/mol) confirms electron delocalization in the heteroatom-containing regions. These results indicate a delocalized electronic structure within the aromatic and heteroatom-containing framework of DMBI, which contributes to its intrinsic electronic stability. However, these electronic features should not be directly interpreted as evidence of biological activity. The σ→σ* and π→π* hyperconjugative transitions observed in the NBO analysis suggest some degree of intramolecular electronic flexibility, which may influence the overall conformational behavior of the molecule. The electronic density provided by π-systems and heteroatoms allows for possible noncovalent interaction sites (e.g., hydrogen bonding and π–π interactions) in a general theoretical sense. It should be emphasized that NBO analysis alone does not provide direct evidence of binding affinity or inhibitory activity against specific protein targets. Therefore, any biological interpretation should be considered in combination with molecular docking and other computational/experimental methods. The F(i,j) coupling integrals of 0.06–0.08 a.u. in π-interactions indicate orbital overlap in these regions.

These values are lower in σ→σ* interactions, consistent with their hyperconjugative character. The observation of high E(2) interactions at low energy differences E(j)–E(i) confirms resonance-assisted stabilization effects within the electronic structure. In conclusion, the NBO results indicate significant π-conjugation, heteroatom-assisted resonance, and hyperconjugative stabilization in the electronic structure of the DMBI molecule. These results suggest a stable and delocalized electronic framework that governs the intrinsic properties of the molecule, particularly its electronic stability and reactivity, rather than directly indicating biological activity.

Table 3. Selected natural bond orbital (NBO) analysis results of the DMBI molecule calculated using the B3PW91 method.

NBO(i)	Type	Occupancies	NBO(j)	Type	Occupancies	E(2)[a] (Kcal/mol)	E (j)-E(i)[b] (a.u.)	F (i, j)[c] (a.u)
C1-C2	π	1.67145	C3-C4	π*	0.38278	16.75	0.28	0.062
C1-C2	π	1.67145	C5-C6	π*	0.37551	21.76	0.29	0.072
C1-C6	σ	1.97909	C5-C9	σ*	0.03084	5.02	1.20	0.069
C2-C3	σ	1.97644	C4-N7	σ*	0.02628	6.54	1.14	0.077
C3-C4	σ	1.97690	C4-C5	σ*	0.02886	4.53	1.27	0.068
C3-C4	π	1.66387	C1-C2	π*	0.34978	22.26	0.29	0.072
C3-C4	π	1.66387	C5-C6	π*	0.37551	16.22	0.30	0.063
C3-H25	σ	1.98086	C4-C5	σ*	0.02886	4.51	1.08	0.063
C5-C6	σ	1.97413	C4-C5	σ*	0.02886	4.37	1.25	0.066
C5-C6	σ	1.97413	C5-C9	σ*	0.03084	4.09	1.21	0.063
C5-C6	π	1.64896	C1-C2	π*	0.34978	18.13	0.28	0.064
C5-C6	π	1.64896	C3-C4	π*	0.38278	23.13	0.28	0.072
C5-C6	π	1.64896	C9-N11	π*	0.23650	17.85	0.27	0.064
C5-C9	σ	1.96548	C3-C4	σ*	0.02233	4.19	1.24	0.065
C5-C9	σ	1.96548	N11-N12	σ*	0.01842	4.20	1.07	0.060
C6-H26	σ	1.98053	C4-C5	σ*	0.02886	4.81	1.07	0.064
N7-C8	σ	1.98742	C3-C4	σ*	0.02233	4.16	1.38	0.068
C8-C9	σ	1.97647	C5-C6	σ*	0.02321	4.37	1.24	0.066
C8-O10	π	1.99598	C9-N11	π*	0.23650	4.89	0.39	0.041
C9-N11	π	1.98770	C5-C6	π*	0.37551	9.98	0.36	0.057
C9-N11	π	1.98770	C8-O10	π*	0.27299	11.45	0.34	0.057
C9-N11	π	1.98770	N12-C13	π*	0.00808	12.36	0.34	0.059
N11-N12	σ	1.97723	C5-C9	σ*	0.03084	4.77	1.31	0.071
N11-N12	σ	1.97723	C13-C14	σ*	0.02581	4.14	1.33	0.066
N12-C13	π	1.83070	C9-N11	π*	0.23650	18.66	0.33	0.072
C13-H28	σ	1.98629	C14-C15	σ*	0.01264	4.37	1.10	0.062
C15-H29	σ	1.97849	C14-C19	σ*	0.02222	4.32	1.08	0.061
C15-H29	σ	1.97849	C16-C17	σ*	0.02345	4.72	1.05	0.063
C16-H30	σ	1.97869	C14-C15	σ*	0.01264	4.14	1.09	0.060
C18-H31	σ	1.97892	C14-C19	σ*	0.02222	4.07	1.10	0.060
C19-H32	σ	1.98034	C14-C15	σ*	0.01264	4.15	1.09	0.060

C19-H32	σ	1.98034	C17-C18	σ*	0.02289	4.45	1.07	0.062
C3-C4	π*	0.38278	C5-C6	π*	0.37551	283.17	0.01	0.081
C8-C9	σ*	0.10184	N11-N12	σ*	0.01842	14.29	0.02	0.061
C9-N11	σ*	0.01406	C5-C6	π*	0.37551	124.00	0.02	0.074

ADMET analysis

ADMET assessments play a critical role in predicting efficacy, safety, and therapeutic potential by comprehensively describing a compound's behavior in biological systems [42]. Understanding these properties allows for optimizing the compound's design and minimizing undesirable effects while effectively reaching the target site. Establishing an appropriate ADMET profile requires that the compound not only exhibit biological activity but also possess the necessary pharmacokinetic properties as a drug candidate [43]. In clinical trials, a balanced ADMET profile is crucial for ensuring adequate bioavailability, optimal distribution to target tissues, efficient metabolism, and appropriate excretion rates [44].

In this study, the ADMET properties of DMBI were evaluated, and the physicochemical and pharmacokinetic parameters presented in Table 4 provide important information regarding the compound's potential behavior in biological systems. According to the table, the structure, which contains a molecular weight of 292.13 Da, five hydrogen bond acceptors, and one hydrogen bond donor, indicates that the compound possesses basic drug-like characteristics. In addition, the molecular weight, logP (3.698), nHA (5), and nHD (1) values of the compound were consistent with Lipinski's Rule of Five, suggesting that the compound may exhibit a potentially favorable profile in terms of oral bioavailability under theoretical conditions [45].

Although the logP value of 3.698 and TPSA of 57.06 Å² reveal a balanced profile in terms of lipophilicity and polar surface area, the extremely low HIA (0.006) and Caco-2 permeability (-4.586) values reported in Table 4 indicate that the compound is likely to exhibit very limited intestinal absorption and membrane permeability under physiological conditions. This suggests a potential limitation for oral bioavailability despite compliance with Lipinski's rule. The BBB penetration value in the same table (0.563) suggests that the compound has a moderate and possibly partial blood-brain barrier penetration potential.

High plasma protein binding (96.20%) and moderate volume of distribution (VD = 0.758) indicate that the free drug fraction in circulation is expected to be limited, which may further reduce systemic exposure. Furthermore, CYP2D6 (0.049) and CYP3A4 (0.529) inhibition values suggest that the compound may exhibit low to moderate interaction with metabolic enzymes, while the short half-life (T1/2 = 0.595) supports a rapid elimination trend, indicating that frequent dosing or formulation strategies may be required to maintain effective concentrations. When the safety parameters are examined, low hERG blockade (0.001), low hepatotoxicity (0.045), and low mutagenicity risk (AMES = 0.926) given in Table 4 indicate that the compound presents a relatively favorable safety profile in silico predictions. However, these results should be interpreted cautiously as they are computational predictions and require experimental validation. The low rat oral acute toxicity value (0.098) also supports this assessment. Furthermore, the structural representation and radar plot presented in Figure 4 allow for visual assessment of the physicochemical and lipophilic properties of the DMBI compound. The structure demonstrates that the compound has a suitable framework in terms of aromatic rings, heteroatoms, and side chain arrangement. The radar plot, which presents critical parameters such as logP, TPSA, nHA, nHD, nRot, and ring number along with their lower and upper acceptance limits, allows for rapid visualization of the overall physicochemical space of DMBI. The compound profile shown in the figure suggests that a general balance between lipophilicity and polar surface area is observed, and that the molecule is also within acceptable ranges in terms of flexibility and ring system. However, despite these favorable physicochemical descriptors, the poor predicted absorption and

permeability values indicate that the overall pharmacokinetic profile should be considered with caution rather than as fully favorable. In this respect, Figure 4 complements the ADMET and physicochemical evaluations presented in Table 4 and contributes to a more comprehensive understanding of the compound's theoretical drug-like profile.

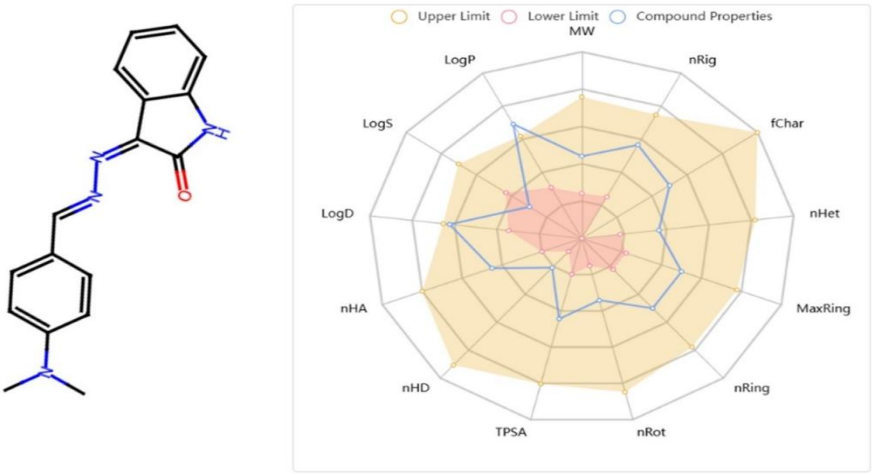


Figure 4. Molecular structure and physicochemical and lipophilicity parameters of the DMBI molecule.

Table 4. Physicochemical, lipophilicity, and ADMET parameters of the DMBI molecule.

Property	DMBI compound	Benchmark / Acceptable range
Molecular weight	292.13	< 500 Da (Lipinski)
nHA	5	≤ 10
nHD	1	≤ 5
logP	3.698	≤ 5
TPSA	57.06	< 140 Å² (Oral absorption)
HIA	0.006	> 0.3 (High absorption)
Caco-2 permeability	-4.586	> -5.15 (Poor–good threshold varies)
BBB	0.563	> 0.3 (BBB permeable)
PPB	96.20%	< 90% Preferred (High binding if > 90%)
VD	0.758	0.6-1.2 L/kg (Typical range)
CYP2D6	0.049	< 0.5 (Low inhibition risk)
CYP3A4	0.529	< 0.5-0.7 (Moderate threshold)
$T_{1/2}$	0.595	> 0.5 h (Very short borderline)
hERG blockers	0.001	< 0.1 (Low risk)
H-HT	0.045	< 0.1 (Low hepatotoxicity)
AMES toxicity	0.926	> 0.8 (Non-mutagenic tendency)
Rat oral acute toxicity	0.098	Low value = Low toxicity

Molecular docking studies

Pharmacological data and drug design studies are critical for understanding the biochemical performance of potential therapeutic compounds [46]. These studies aim to elucidate the efficacy, mechanism of action, and therapeutic potential of drugs by examining their interactions with

biological targets, particularly proteins [47]. The classification of protein–ligand interactions, defined as the binding of a ligand to a specific protein target such as an enzyme or receptor, constitutes the basis of drug biological activity. Molecular docking is a computer-based technique that models the interactions between ligands and target proteins at the molecular level [48]. The main objective is to identify energetically favorable binding conformations, which may provide insight into binding affinity within the limits of computational scoring functions. In this context, identifying potential inhibitors against tuberculosis (TB) is of significant interest, particularly for *Mycobacterium tuberculosis* target enzymes [49]. In this study, the interaction potential of DMBI on TB target proteins was investigated using molecular docking analyses. Docking studies were performed with AutoDock Vina software and the resulting ligand-protein complexes were visualized and evaluated in detail with 3-[(E)-2-(4-phenyl visualizer. Within the scope of the analyses, the interactions of DMBI with the enzymes PDB: 1SJ2 and PDB: 4P8N were investigated comparatively with the relevant control ligands. For PDB: 1SJ2, 3-[18-(2-carboxyethyl)-8,13-bis(ethenyl)-3,7,12,17-tetramethylporphyrin-21,23-diid-2-yl]propanoic acid was used as the control ligand; Iron(2+) was used for control ligand 1, and 3-[(3-fluoro-4-methoxybenzyl)amino]-6-(trifluoromethyl)quinoxaline-2-carboxylic acid (control ligand 2) was used for PDB: 4P8N and shown in Figure 5a, 5b. The docking scores obtained indicate that DMBI has significant binding potential on both enzymes. In particular, the -8.1283 score obtained with PDB: 4P8N is quite close when compared to the control ligand (-9.1459), suggesting that DMBI can effectively interact with the target protein. The -9.7859 score obtained with PDB: 1SJ2, although slightly weaker than the control ligand (-10.8348), may be associated with different binding modes or the flexible nature of the molecule; this suggests that DMBI could be a suitable candidate for structural optimization studies. In addition, the RMSD values (1.3212–1.6584 Å) confirm that the docked pose of DMBI is compatible and stable with the target protein. Overall, these findings support that DMBI may exhibit biologically relevant interactions with both PDB: 1SJ2 and PDB: 4P8N enzymes and may be considered a potential inhibitor candidate. Therefore, DMBI exhibits strong binding to target proteins compared to selected control ligands, making it a promising candidate for further biological validation and structural optimization studies in the treatment of tuberculosis. Molecular docking analyses reveal the interaction mechanisms of DMBI with the TB target proteins PDB:1SJ2 and PDB:4P8N in detail. The interactions of DMBI with 1SJ2 are summarized in Table S3. The analyses indicate that DMBI interacts with amino acids such as PHE-252, HIS-270, THR-275, HIS-276, and SER-315 through van der Waals interactions. Additionally, a carbon-hydrogen bond was detected with ARG-104 at a distance of 3.82 Å, Pi-Pi stacked interactions were detected with TRP-107 at a distance of 4.44 Å, and Pi-Pi T-shaped interactions were detected with TRP-321 at a distance of 7.78 Å. Alkyl and Pi-Alkyl bonds were formed with residues such as LEU-415, LEU-265, ILE-103, PRO-232, LEU-378, and ARG-104. Compared to the control ligand, the multiple interaction types and favorable bond distances of DMBI indicate that the molecule assumes a stable position on 1SJ2 and can bind strongly to the target protein. Similarly, the interactions of DMBI with the 4P8N enzyme have been detailed in Table S4. DMBI formed Van der Waals interactions with ASN-324, HIS-315, GLY-117, LEU-363, and SER-228, while it formed conventional hydrogen bonds with LYS-418, CYS-387, and GLN-336. Pi-Pi stacked and Pi-Pi T-shaped interactions were observed with FAD-501 residues, and alkyl and Pi-Alkyl bonds were also observed with LEU-317, ARG-325, VAL-365, and LYS-367 and shown in Figure 5c, 5d. Compared to the control ligand 2, DMBI exhibited multiple binding sites and appropriate bond distances, indicating that it effectively positions itself in the active site of the enzyme . These interaction profiles support the biologically significant binding potential of DMBI on both 1SJ2 and 4P8N enzymes and suggest that it could be considered a potential inhibitor candidate for the treatment of tuberculosis.

Table 5. Molecular docking interactions scores with PDB: 1SJ2, PDB: 4P8N enzymes of the DMBI compound and control ligands.

	PDB: 1SJ2		PDB: 4P8N	
	DMBI	Control ligand 1	DMBI	Control ligand 2
Docking score	-9.7859	-10.8348	-8.1283	-9.1459
RMSD values	1.6584	0.3883	1.3212	0.4703

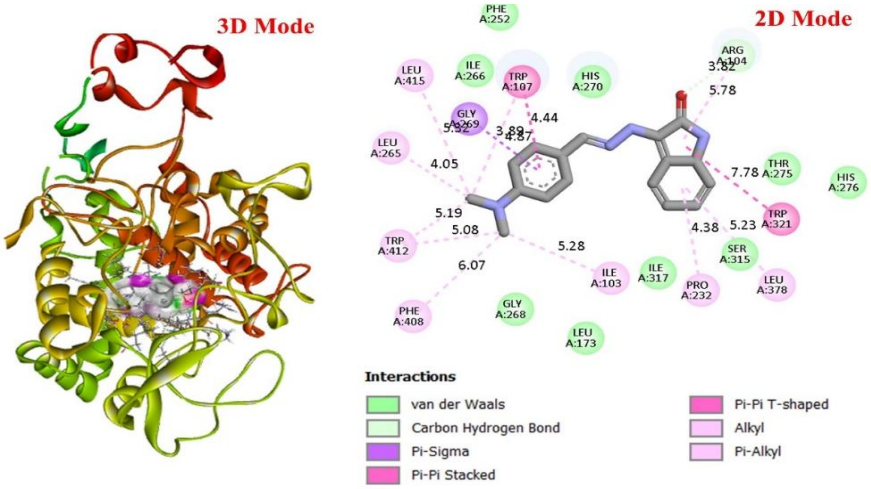


Figure 5a. Three-dimensional (3D) and two-dimensional (2D) representations of the DMBI compound and the PDB: 1SJ2 protein.

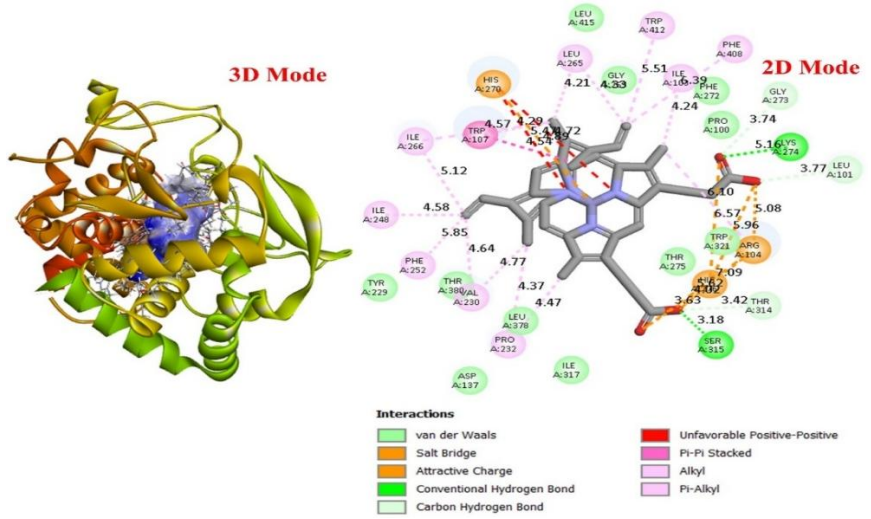


Figure 5b. Three-dimensional (3D) and two-dimensional (2D) representations of the control ligand 1 and the PDB: 1SJ2 protein.

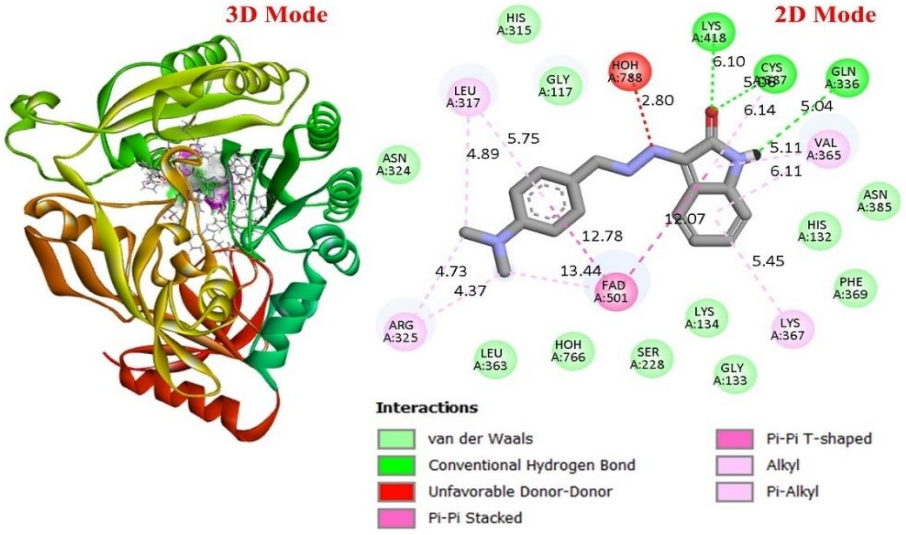


Figure 5c. Three-dimensional (3D) and two-dimensional (2D) representations of the DMBI compound and the PDB: 4P8N protein.

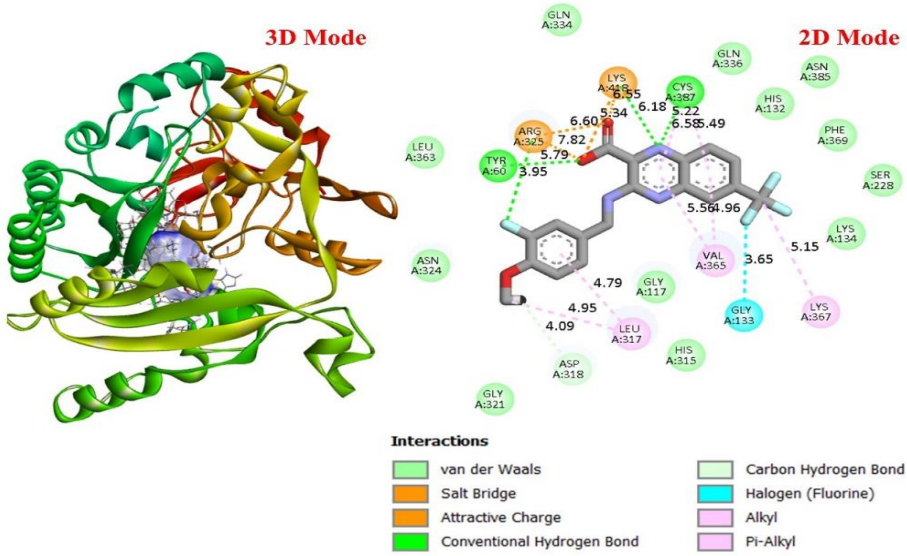


Figure 5d. Three-dimensional (3D) and two-dimensional (2D) representations of the control ligand 2 and the PDB: 4P8N protein.

CONCLUSION

In this study, the potential inhibitory activity of the Schiff base derivative DMBI against tuberculosis target enzymes was investigated using an integrated approach that combines computational chemistry methods, molecular docking analyses, and ADMET evaluations. DFT

calculations demonstrated that DMBI has a stable electronic structure, a favorable HOMO–LUMO energy range, and a planar geometry consistent with literature. MEP and Mulliken charge analyses revealed distinct electrophilic and nucleophilic regions in the compound, suggesting possible reactive centers that may contribute to protein–ligand interactions. NBO analysis revealed the presence of strong $\pi \rightarrow \pi^*$ delocalization in the aromatic backbone and heteroatom-containing segments, which was found to contribute to the conjugative stability of the molecule. The high dipole moment, polarizability, and hyperpolarizability values indicate notable electronic response characteristics, suggesting that these properties may be relevant to its interaction with biological systems rather than directly implying biological activity. Molecular docking results revealed that DMBI exhibits moderate to good predicted binding affinity for *Mycobacterium tuberculosis* enzymes (PDB: 1SJ2 and 4P8N) and is stably located in the active site. The binding modes are predominantly based on hydrophobic contacts and π-alkyl interactions, which may indicate potential for further optimization toward improved binding affinity. ADMET analyses revealed that DMBI possesses drug-like properties and a relatively safe toxicity profile; however, limitations in absorption and metabolic stability suggest that further optimization is required. Overall, the computational results suggest that DMBI could be considered as a preliminary scaffold for tuberculosis inhibitor development, rather than a fully validated candidate. Structural modifications and experimental validation studies to improve the molecule's pharmacokinetic properties are strongly recommended for future research. This study demonstrates that DMBI may serve as a useful starting point in anti-tuberculosis drug design efforts.

Conflicts of interest

The authors declare no conflicts of interest.

Data availability statement

The data that support the findings of this study are available from the corresponding author upon reasonable request.

Funding: The authors declare that they received no financial support.

REFERENCES

1. Edet, H.O.; Louis, H.; Gber, T.E.; Idante, P.S.; Egemonye, T.C.; Ashishie, P.B.; Oyo-Ita, E.E.; Benjamin, I.and, Adeyinka, A.S. Heteroatoms (B, N, S) doped quantum dots as potential drug delivery system for isoniazid: insight from DFT, NCI, and QTAIM. *Heliyon* **2023**, 9, e12599.
2. Bağlan, M.; Gören, K.and, Yıldıko, Ü. HOMO–LUMO, NBO, NLO, MEP analysis and molecular docking using DFT calculations in DFPA molecule. *IJCT.* **2023**, 7, 38-47.
3. Kutlu, E.; Emen, F.M.; Yıldırım, K.; Ataş, C.; Demirdogen, R.E.; Yesilkaynak, T.; Kinaytürk, N.K.; Şimşek, E.and, Çoban, A.Y. Novel thiourea derivatives against *Mycobacterium tuberculosis*: Synthesis, characterization and molecular docking studies. *Phosphorus Sulfur Silicon Relat. Elem.* **2023**, 198, 844-853.
4. Nyijime, T.A.; Shallangwa, G.A.; Uzairu, A.; Umar, A.B.; Ibrahim, M.T.and, Al-Amin, M.D. Identification of Potential anti-tubercular inhibitors through virtual screening, DFT, and molecular dynamics simulation studies. *Curr. Pharm. Anal.* **2026**, 22, 23-34.
5. Gören, K.; Kotan, G.; Manap, S. and Yüksek, H. Synthesis, antimicrobial and antioxidant activities of 3-alkyl(aryl)-4-(3-methoxy-4-hydroxybenzylideneamino)-4,5-dihydro-1h-1,2,4-triazol-5-one derivatives. *Chem. Afr.* **2024**, 7, 5273-5289.

6. Alyar, S.; Şen, T.; Özmen, Ü.Ö.; Alyar, H.; Adem, Ş.and, Şen, C. Synthesis, spectroscopic characterizations, enzyme inhibition, molecular docking study and DFT calculations of new Schiff bases of sulfa drugs. *J. Mol. Struct.* **2019**, 1185, 416-424.
7. Noureldeen, A.F.H.; Aziz, S.W.; Shouman, S.A.; Mohamed, M.M.; Attia, Y.M.; Ramadan, R.M.and, Elhady, M.M. Molecular design, spectroscopic, DFT, pharmacological, and molecular docking studies of novel ruthenium(III)–Schiff base complex: An inhibitor of progression in HepG2 cells. *Int. J. Environ. Res. Public Health* **2022**, 19, 2-3.
8. Abdulaziz, L.; Elhadi, E.; Abdallah, E.A.; Alnoor, F.A.and, Yousef, B.A. Antiviral activity of approved antibacterial, antifungal, antiprotozoal and anthelmintic drugs: Chances for drug repurposing for antiviral drug discovery. *J. Exp. Pharmacol.* **2022**, 14, 97-115.
9. Raza, M.A.; Dege, N.; DoĞAn, O.E.; AĞAr, T.and, Sumrra, S.H. Synthesis of two new Schiff bases; crystal structure, Hirshfeld surface analysis, density functional theory and molecular docking. *J. Mol. Struct.* **2021**, 1226, 8-9.
10. Bağlan, M.; Gören, K.and, Çakmak, İ. Theoretical investigation of ^{1}H and ^{13}C-NMR spectra of diethanol amine dithiocarbamate RAFT agent. *J. Inst. Sci. Technol.* **2022**, 12, 1677-1689.
11. Ramalingam, A.; Sambandam, S.; Medimagh, M.; Al-Dossary, O.; Issaoui, N.and, Wojcik, M.J. Study of a new piperidone as an anti-Alzheimer agent: Molecular docking, electronic and intermolecular interaction investigations by DFT method. *J. King Saud Univ. Sci.* **2021**, 33, 10-11.
12. Hagar, M.; Ahmed, H.A.; Aljohani, G.and, Alhaddad, O.A. Investigation of some antiviral n-heterocycles as COVID 19 drug: Molecular docking and DFT calculations. *Int. J. Mol. Sci.* **2020**, 21, 5-6.
13. Mermer, A.; Bayrak, H.; Alyar, S.and, Alagumuthu, M. Synthesis, DFT calculations, biological investigation, molecular docking studies of β-lactam derivatives. *J. Mol. Struct.* **2020**, 1208, 127891.
14. Amul, B.; Muthu, S.; Raja, M.and, Sevvanthi, S. Spectral, DFT and molecular docking investigations on Etodolac. *J. Mol. Struct.* **2019**, 1195, 747-761.
15. Garkusha, N.A.; Anikeeva, O.P.; Bayıl, I.; Taskin-Tok, T.and, Safin, D.A. DFT, ADMET, molecular docking and molecular dynamics studies of pyridoxal. *J. Indian Chem. Soc.* **2023**, 100, 100926.
16. Dekir, A.; Berredjem, M.; Rachedi, K.O.; Bahadi, R.; Djouad, S.E.; Bouacida, S.; Grib, I.; Iqbal, N.; Redjemia, R.and, Boussaker, M. X-ray crystallographic study, molecular docking, molecular dynamics and DFT/ADMET analyses of carboxylsulfamides. *J. Mol. Struct.* **2023**, 1289, 135831.
17. Gupta, D.; Pathak, D.; Kapoor, G.and, Bhutani, R. A Comprehensive review on synthesis and biological activity of Schiff bases. *Int. Res. J. Pharm.* **2019**, 10, 1-8.
18. Frisch, M.J.T., G. W.; Schlegel, H. B.; Scuseria, G. E.; Robb, M. A.; Cheeseman, J. R.; Scalmani, G.; Barone, V.; Mennucci, B.; Petersson, G. A.; Nakatsuji, H.; Caricato, M.; Li, X.; Hratchian, H. P.; Izmaylov, A. F.; Bloino, J.; Zheng, G.; Sonnenberg, J. L.; Hada, M.; Ehara, M.; Toyota, K.; Fukuda, R.; Hasegawa, J.; Ishida, M.; Nakajima, T.; Honda, Y.; Kitao, O.; Nakai, H.; Vreven, T.; Montgomery Jr., J. A.; Peralta, J. E.; Ogliaro, F.; Bearpark, M. J.; Heyd, J. J.; Brothers, E.; Kudin, K. N.; Staroverov, V. N.; Kobayashi, R.; Normand, J.; Raghavachari, K.; Rendell, A. P.; Burant, J. C.; Iyengar, S. S.; Tomasi, J.; Cossi, M.; Rega, N.; Millam, J. M.; Klene, M.; Knox, J. E.; Cross, J. B.; Bakken, V.; Adamo, C.; Jaramillo, J.; Gomperts, R.; Stratmann, R. E.; Yazyev, O.; Austin, A. J.; Cammi, R.; Pomelli, C.; Ochterski, J. W.; Martin, R. L.; Morokuma, K.; Zakrzewski, V. G.; Voth, G. A.; Salvador, P.; Dannenberg, J. J.; Dapprich, S.; Daniels, A. D.; Farkas, Ö.; Foresman, J. B.; Ortiz, J. V.; Cioslowski, J.; Fox, D. J., *Gaussian 09*. 2009.
19. Eberhardt, J.; Santos-Martins, D.; Tillack, A.F.and, Forli, S. AutoDock Vina 1.2.0: New docking methods, expanded force field, and python bindings. *J. Chem. Inf. Model.* **2021**, 61, 3891-3898.

20. Bertrand, T.E., N. A. J.; Jones, J. N.; Bodiguel, J.; Jesmin; Nagy, J. M.; Raven, E. L.; Jamart-Gregoire, B.; Brown, K. A. *1SJ2 – Crystal structure of Mycobacterium tuberculosis catalase-peroxidase*. **2024**, [cited 2025 29.11.2025]; Available from: https://www.rcsb.org/structure/1SJ2.
21. Neres, J.P., F.; Cole, S. T. *4P8N – Crystal structure of M. tuberculosis DprE1 in complex with non-covalent inhibitor QN118*. **2014**, [cited 2025 29.11.2025]; Available from: https://www.rcsb.org/structure/4P8N.
22. Dassault Systèmes BIOVIA. Discovery studio modeling environment, Release 2016; Dassault Systèmes: San Diego, CA, USA, **2016**.
23. ADMETlab 2.0: A platform for systematic ADMET evaluation. [cited 2025 29.11.2025]; Available from: https://admetlab2.scbdd.com.
24. Bağlan, M.; Gören, K.and, Yıldıko, Ü. DFT Computations and molecular docking studies of 3-(6-(3-aminophenyl)thiazolo[1,2,4]triazol-2-yl)-2h-chromen-2-one(ATTC)molecule. *Hittite J. Sci. Eng.* **2023**, 10, 11-19.
25. Bağlan, M.; Yıldıko, Ü.and, Gören, K. Computational investigation of 5.5",7"-trihydroxy-3,7-dimethoxy-4'-4"'-O-biflavone from flavonoids using DFT calculations and molecular docking. *Adıyaman Univ. J. Sci.* **2022**, 12, 283-298.
26. Jamal Ara, R.; Ashiq, U.; Yousuf, S. (3Z)-3-Hydrazinylideneindolin-2-one. *Acta Crystallogr. Sect. E Struct. Rep. Online.* **2011**, 67, o2576.
27. Halasangi, B.M.; Badami, P.S.; Patil, S.A.and, Anil Kumar, G.N. Crystal structure of 3-[(E)-2-(4-phenyl-1,3-thia-zol-2-yl)hydrazin-1-yl-idene]indolin-2-one. *Acta Crystallogr. Sect. E Struct. Rep. Online.* **2014**, 70, o1177- o11778.
28. Eldehna, W.M.; Abo-Ashour, M.F.; Ibrahim, H.S.; Al-Ansary, G.H.; Ghabbour, H.A.; Elaasser, M.M.; Ahmed, H.Y.A.and, Safwat, N.A. Novel [(3-indolylmethylene)hydrazono]indolin-2-ones as apoptotic anti-proliferative agents: design, synthesis and in vitro biological evaluation. *J. Enzyme Inhib. Med. Chem.* **2018**, 33, 686-700.
29. Bağlan, M.; Yıldıko, Ü.and, Gören, K. DFT calculations and molecular docking study in 6-(2"-Pyrrolidinone-5"-Yl)-(-) epicatechin molecule from flavonoids. *Eskişehir Teknik Üniversitesi Bilim ve Teknoloji Dergisi B - Teorik Bilimler.* **2023**, 11, 43-55.
30. Çimen, E.; Gören, K.; Tahiroğlu, V.and, Yıldıko, Ü. The theoretical calculations by DFT method and analysis ADME, molecular docking of 1-(1-(4-hydroxybutyl)-6-methyl-4-phenyl-2-thioxohexahydropyrimidin-5-yl)ethan-1-one (pyrimidine-thiones) compound. *OKÜ Fen Bil. Ens. Dergisi.* **2025**, 8, 1129-1145.
31. Gören, K.; Bağlan, M.; Tahiroğlu, V.and, Yıldıko, Ü. Theoretical calculations and molecular docking analysis of 4-(2-(4-bromophenyl)hydrazineylidene)-3,5-diphenyl-4H-pyrazole molecule. *J. Adv. Res. Nat. Appl. Sci.* **2024**, 10, 786-802.
32. Huang, Y.; Rong, C.; Zhang, R.and, Liu, S. Evaluating frontier orbital energy and HOMO/LUMO gap with descriptors from density functional reactivity theory. *J. Mol. Model.* **2016**, 23, 3.
33. Gören, K.; Bağlan, M.and, Yıldıko, Ü. Antimicrobial, and antitubercular evaluation with ADME and molecular docking studies and DFT calculatıons of (Z)-3-((1-(5-amino-1,3,4-thiadiazol-2-yl)-2-Phenylethyl)imino)-5-nitroindolin-2-one Schiff base. *Karadeniz Fen Bilim. Derg.* **2024**, 14, 1694-1708.
34. Gören, K.; Bağlan, M.and, Yıldıko, Ü. Melanoma cancer evaluation with ADME and molecular docking analysis, DFT calculations of (e)-methyl 3-(1-(4-methoxybenzyl)-2,3-dioxoindolin-5-yl)-acrylate molecule. *J. Inst. Sci. Technol.* **2024**, 14, 1186-1199.
35. Chatterjee, S.; Afzal, M.; Mandal, P.C.; Modak, R.; Guin, M.and, Konar, S. Exploration of supramolecular interactions, Hirshfeld surface, FMO, molecular electrostatic potential (MEP) analyses of pyrazole based Zn (II) complex. *J. Indian Chem. Soc.* **2024**, 101, 101275.

36. Gören, K.; Bağlan, M.and, Yıldıko, Ü. Analysis by DFT, ADME and docking studies of N'-(4-Hydroxy-3-Methoxybenzylidene)Naphtho[2,3-B]Furan-2-carbohydrazide. *Eskişeh. Tek. Univ. Bilim Teknol. Derg. Teor. Bilim.* **2025**, 13, 7-23.
37. Çimen, E.; Gören, K.; Tahiroğlu, V.and, Bağlan, M. Chemical reactivity, molecular docking and ADMET profile of (E)-4-((2-butyl-5-(2-carboxy-3-(thiophen-2-yl) prop-1-en-1-yl)-1 H-imidazol-1-yl) methyl) benzoic acid molecule: evaluation as a diabetes drug candidate. *J. Iran. Chem. Soc.* **2026**, 23, 46.
38. Tahiroğlu, V.; Gören, K.and, Bağlan, M. *In silico* drug evaluation by molecular docking, ADME studies and DFT calculations of 2-(6-chloro-2-(4-chlorophenyl)imidazo[1,2-a]pyridin-3-yl)-N, N-dipropylacetamide. *BMC Pharmacol. Toxicol.* **2025**, 26, 116.
39. Tahiroğlu, V.; Gören, K.; Bağlan, M.and, Yıldıko, Ü. Molecular docking and DFT analysis of thiazolidinone-bis Schiff base for anti-cancer and anti-urease activity. *J. Inst. Sci. Technol.* **2024**, 14, 822-834.
40. Tahiroğlu, V.; Gören, K.; Çimen, E.and, Yıldıko, Ü. Molecular docking and theoretical analysis of the (e)-5-((z)-4-methylbenzylidene)-2-(((e)-4-methylbenzylidene)hydrazineylidene)-3-phenylthiazolidin-4-one molecule. *Bitlis Eren Üniv. Fen Bilim. Derg.* **2024**, 13, 659-672.
41. Mazyed, H.A.K.; Imran, N.H.; Mohammed, S.A.; Munahi, M.G.and, Nahi, R.J. Computational details of molecular structure, spectroscopic properties, DFT calculations and molecular docking study of some 1, 4-disubstituted-1, 2, 3-triazole derivatives derived from 4-aminobenzen sulfonic acid. *Bull. Chem. Soc. Ethiop.* **2025**, 39, 585-600.
42. Tahiroğlu, V.; Gören, K.; Yıldıko, Ü.and, Bağlan, M. Investigation, structural characterization and evaluation of the biological potency by molecular docking of amoxicillin analogue of a Schiff base molecule. *Int. J. Chem. Technol.* **2024**, 8, 190-199.
43. Bağlan, M.; Gören, K.; Tahiroğlu, V.; Kotan, G.; Manap, S.and, Yüksek, H. Design, synthesis, DFT-Based Characterization, molecular docking, and ADMET evaluation of a novel mannich base derivative. *ChemistrySelect.* **2026**, 11, e06617.
44. Abchir, O.; Yamari, I.; Nour, H.; Daoui, O.; Elkhattabi, S.; Errougui, A.and, Chtita, S. Structure-based virtual screening, ADMET analysis, and molecular dynamics simulation of moroccan natural compounds as candidates α-amylase inhibitors. *Chem. Select.* **2023**, 8, e202301092.
45. Lipinski, C.A.; Lombardo, F.; Dominy, B.W.and, Feeney, P.J. Experimental and computational approaches to estimate solubility and permeability in drug discovery and development settings. *Adv. Drug Deliv. Rev.* **1997**, 23, 3-25.
46. Kotan, G.; Gören, K.; Manap, S.; Bağlan, M.and, Yüksek, H. Novel Mannich bases based on schiff bases: Synthesis, biological activities, computational approach, and anticancer analysis with molecular docking. *Acta Chim. Slov.* **2025**, 72, 637.
47. Adelina, R. Simulasi docking molekuler senyawa potensial tanaman justicia gendarussa *Burm. f.* Sebagai antidiabetes molecular docking simulation of justicia gendarussa as antidiabetic. *Bull. Health Res.* **2020**, 48, 117-122.
48. Gören, K.and, Yıldıko, Ü. Aldose reductase evaluation against diabetic complications using ADME and molecular docking studies and DFT calculations of spiroindoline derivative molecule. *Süleyman Demirel Univ. Fen Bilim. Enst. Derg.***2024**, 28, 281-292.
49. Agbektas, T.; Coskun, H.; Genc, H.C.; Cinar Kaya, G.; Tas, A.; Goren, K.; Huseynzada, A.; Guliyev, R.; Hasanova, U.and, Kaya, S. Evaluation of the anticancer effects of DODP on gene expression and oxidative stress in gastric cancer: An integrated docking, bioinformatics, and experimental approach. *Life* **2026**, 16, 534.